Measuring Topological Properties of Dynamical Systems

Connor Duncan*

November 9, 2021

*Partner: Glenn LeBlanc. From Dune: "the spice must flow." Also worth noting, all of the Figures are hyperlinked, and a few of them are put at the end due to formatting constraints.

Contents

1 Theoretical Background **2**
1.1 Dynamical Systems . . . 2
1.1.1 Dynamical Flow and Phase Space . . . 3
1.1.2 Time-Delay Embedding . . . 4
1.2 Chaos in Dynamical Systems . . . 5
1.2.1 Lyapunov Stability . . . 5
1.2.2 Bifurcation and Universal Behavior . . . 6
1.2.3 Attractor Dimension . . . 7

2 Experimental Apparatus **9**
2.1 PN-Junction . . . 10
2.2 Bouncing Ball . . . 11
2.3 Sources of Error in Dimension . . . 12

3 Conclusion **13**

A Code **14**

1 Theoretical Background

The study of dynamical systems is grounded deeply in the type of analysis (in the literal, mathematical sense) that I so masochistically enjoy. While physicists (especially in undergraduate laboratory work) tend to gloss over the finer details, there are several theorems and concepts which, with appropriate definition, simplify the measurement procedure for the apparatuses described in Section 2, and more importantly, are very cool in their own right. In what follows, I will introduce some concepts from mathematics which are used throughout the study of Dynamics, and attempt to provide some basic intuition for their utility.[1] Particular attention will be paid to Takens' theorem, which establishes an embedding between Phase-Space manifolds and time-delay coordinates, and to estimation methods for the self-similarity of phase orbits. A discussion of potential errors can be found in Section 2.

1.1 Dynamical Systems

At a very high level, a dynamical system is a formal description the the *state* of some system as it changes with time. In the most general form, this is represented by a 3-tuple, consisting of: T, an additive monoid (associative, with an identity), usually a subset of $\mathbb{R}$ or $\mathbb{Z}$, which represents an evolution parameter (usually called *time*); $\mathcal{M}$, a set consisting of all possible system configurations (usually called *state* or *configuration* space); and $\varphi : T \times \mathcal{M} \to \mathcal{M}$, a function describing the evolution of points in $\mathcal{M}$. [5] While this formulation is extremely general, it is not well suited to the systems studied in this lab. For our purposes, it will be more convenient to consider two distinct, but related classes of dynamical systems: discrete, and continuous.

[1] At the level of an late-undergraduate physics major who hasn't seen this material explicitly in other coursework. I *strongly* recommend at least checking out Folland if you like Analysis, and Arnold if you like Classical Mechanics (and a little analysis). In addition, the cited papers of Takens and Yorke, Sauer and Casdagli were fun to read, and shed a lot of light on the mathematical mechanics of this lab.

Discrete dynamical systems maybe considered by taking T in following discussion to be discrete, and entirely relaxing differentiability requirements.

1.1.1 Dynamical Flow and Phase Space

To narrow our discussion of dynamical systems into a more familiar realm, we begin first with a familiar class of equations: first order differential equations. It is worth noting that all of the discussion below maps neatly onto differentiable manifolds by taking coordinate charts of the equations, applying the chain rule, and replacing $\mathbb{R}^n$ with the cotangent space at x.[2] Let U be an open subset of $\mathbb{R}^n$, with $x \in U$. Likewise, allow $F : \mathbb{R} \times U \to \mathbb{R}^n$ to be a vector-valued equation (a vector *field*) on $\mathbb{R} \times U$. Then the equation

$$\frac{dx}{dt} = F(t, x) \tag{1}$$

is called the *differential equation* of F, and has solutions of the form $\phi : (a, b) \subset \overline{\mathbb{R}} \to U$[3] such that

$$\left.\frac{d\phi}{dt}\right|_{t=\tau} = F(\tau, \phi(\tau)) \tag{2}$$

for any $\tau \in (a, b)$. This certainly looks like a dynamical system, since $\mathbb{R}$ is a monoid, and our equations are constructed so that U is the space of all possible points reached by any trajectory. To formalize this, we introduce the concept of a *flow* on the state space.

Definition 1 (State Flow)**.** A one parameter group g^t of diffeomorphisms of a domain U is the map of $\mathbb{R} \times U$ into U, $g : \mathbb{R} \times U \to U$, where $g(t, x) = g^t(x)$, for $t \in \mathbb{R}$, $x \in U$ such that

- g is differentiable.
- $\{g^t | t \in \mathbb{R}\}$ preserves the additive structure of $\mathbb{R}$, that is: $g^t \circ g^s = g^{t+s}$, and g^0 is the identity.

A state flow on U is such a one-parameter group of diffeomorphisms.

When considering the behavior of solution spaces of differential equations, characterizing their solutions as phase flows is a useful technique permitting the application of many theorems from topology. A proof that such a characterization is possible may be found in Chapter 2 of *Ordinary Differential Equations*. [2], We make the identification of the solution from Equation 2 with a phase flow by writing $\phi(t) = g^t(x_0)$. Then clearly, the equation of motion of the point x_0 under g is a solution of Equation 1.

Finally, we introduce *phase space*. Succinctly put, phase space may be considered the cotangent bundle of configuration space.[4,5] For our purposes, it is sufficient to regard the phase space of the state space U as $T^*U = \{(x, v) | x \in U, v \in (T_xU)^*\}$, treating every possible tangent vector to x as its own "momentum", and

[2] This is relevant when studying the global topological properties of positive limit sets, which is not something we do in much detail here.

[3] $\overline{\mathbb{R}}$ is the real line $\mathbb{R} \cup \{-\infty, \infty\}$, if this notation isn't familiar.

[4] We choose the cotangent bundle as opposed to the tangent bundle since it gives nice symplectic structure on phase space. I am grateful to Prof. Ivan Danilenko for his insight into the distinction.

[5] Further details regarding (co)tangent bundles may be found in any textbook regarding differential topology (e.g. [6]).

considering the new object as a manifold of dimension twice that of U. It is essentially the space of "initial conditions" of the state flow, since the first derivative at $t = 0$ is also needed to specify solutions to Equation 1.

1.1.2 Time-Delay Embedding

A rather serious problem arises when studying chaotic dynamical systems in a physical setting: in order to characterize phase space, we ought to know the value of every coordinate in configuration space along our trajectory. This poses a problem for experimental physics, since in many cases, it is only practical (or even possible) to measure one or two quantities simultaneously. To resolve this potential catastrophe, we make use of the method of *time delay embedding*, first introduced by Floris Takens in 1980. [10] In this section, I will introduce the mechanics of the time-delay embedding procedure, and try to provide some intuition for its rather elegant topological justification. In order to accomplish this, we require two ingredients: a precise definition of *embedding*, and a weak version of the Whitney Embedding Theorem.

In order to define embedding, we must first define *immersion*. An immersion, loosely speaking, is a smooth map between manifolds $f : M \to N$ such that df_x is injective for every $x \in M$. For our purposes, it is enough to consider M, N to be subsets of $\mathbb{R}^m, \mathbb{R}^n$ respectively, where $\dim M = m$, and $\dim N = n$. The condition that df_x is injective is simply the statement that the image of df_x is of dimension m. This immediately means that if $n < m$, it is impossible to construct an immersion from M into N, since df_x can have dimension at most n, which is strictly less than m. An embedding is an immersion which is also proper, and injective. The condition that an embedding $f : M \to N$ is proper says that if $C \subset N$ is compact (closed and bounded), then $f^{-1}(C) \subset M$ is also compact. Embeddings are sought after because they do not allow self intersection (by injectivity). This, with the addition of the compactness condition implies that every embedding $f : M \to N$ is a diffeomorphism (invertible, smooth in both directions) onto $f(M)$. [3, 6]

The natural question which follows is to ask what the lowest dimensional $\mathbb{R}^n$ we can embed any M of dimension m into is. A full understanding of this requires a bit more topology than there is room for in this exposition.[6] It is a well-established[7] theorem that the lowest dimension for which such an embedding can be guaranteed is $2m$. However, the embedding in $2m$ is generally difficult to find, and for this reason, we weaken the result to $2m + 1$, and illustrate the proof with a heuristic argument. For a self intersecting curve in $\mathbb{R}^2$, it is easy to remove the self-intersection with an arbitrarily small perturbation by introducing a third dimension, orthogonal to the plane of the curve, and perturbing one branch of the intersection into the new direction, as shown in Figure 1.

This is essentially the argument which Takens gives in his 1980 proof of the method of time-delay embedding for dynamical systems with one observable. Takens' broad argument is that for any manifold M

[6] The interested reader is directed to Section 1.8 and Chapter 2 of *Differential Topology* (specifically the discussion of the Whitney Embedding Theorem and Transversality). [6]

[7] The Whitney Embedding Theorem. Proofs of the Whitney embedding theorem, in addition to a generalized form of Takens theorem which makes statements about the number of functions which do not satisfy the theorem for certain contexts may be found in *Embedology*. [12]

of dimension m, with flow ϕ and $y : M \to \mathbb{R}$ a smooth function, it is a generic[8] property that the map

$$\Phi_{\phi,y}(x) = (y(x), y(\phi(x)), \dots y(\phi^{2m}(x))$$

is an embedding. [10] Since Φ is an embedding, it is possible to construct Φ^{-1}, and thus reconstruct the original dynamical system from a trajectory in $\mathbb{R}^{2m+1}$. Of even more utility, however, is that topological invariants of the system (such as dimension and period number) are preserved under this homeomorphism. So, quantities measured in $2m + 1$ delay coordinates for a single observable will be the same as those measured for m coordinates of all observables. If we consider the special case where y is the projection operator of our phase space to a single observable, for samples which are spaced apart by τ, the map $\Phi(x) = (x(t - 2m\tau), x(t - (2m - 1)\tau), \dots x(t))$ is an such an embedding.

1.2 Chaos in Dynamical Systems

We now turn to chaos. What is it, and how can we quantify it? In the following pages, we present some basic methods and concepts which quantify different aspects of chaos. We begin with a derivation of the notion of Lyapunov stability and Lyapunov exponents, which characterize the degree to which pairs of points in phase space remain near to each other under evolution. Using this notion, we will then describe the bifurcation route to chaos, which quantifies the proliferation of Lyapunov stable neighborhoods, describing its relationship to the Fourier transform, and noting several constants which are endemic to *every* chaotic system (provided they are unimodal and 1-dimensional). Finally, we will discuss the dimension of phase orbits under different conditions on the evolution equation, and find that contrary to our intuition, the dimension (appropriately defined) of a trajectory in phase space may in fact be greater than 1, despite the fact that it is a 1-parameter curve.

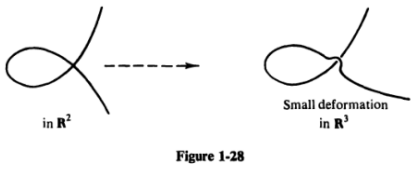

Figure 1: An example of removing a self-intersection by perturbation in the $2m + 1$ dimension. [6, pg. 50]

1.2.1 Lyapunov Stability

Let $D \subset \mathbb{R}^{2n}$ be the phase space corresponding to the evolution equation in 1, with flow ϕ. Consider some ϵ-ball about $\xi \in D$, $B_\epsilon(\xi) = \{\chi \in D | |\xi - \chi| < \epsilon\}$. For a sufficiently small ball, we may consider the linearization of ϕ about ξ from the definition of the derivative of a manifold, to be

$$\tilde{\phi}(\chi) = \phi(\xi) + d\phi_\xi(\xi - \chi) + O(|\epsilon|^2)$$

[8] True outside a set of measure 0.

In this case $d\phi_\xi$ is the Jacobian matrix of first partial derivatives evaluated at ξ (a proof of this may be found in Chapter 1 of *Differential Topology* [6]). Then, for the linearized equation, two points χ, ξ which are ϵ distant from each other evolve by repeated application of $\tilde{\phi}^\delta$. In particular, because we have linearized our equation, the overall flow $\tilde{\phi}$ is given by the matrix exponential.[9] [2, pg. 19]

$$\tilde{\phi}^t(\xi - \chi) = e^{d\phi^t_{\xi(0)}t}(\xi - \chi)$$

Thus, the radius of B_ϵ grows as

$$|\tilde{\phi}^t(\xi - \chi)| \leq |e^{d\phi_{\xi(0)}t}|\epsilon$$

If we choose $d\phi_\xi$ to be diagonalized, then the preceding formula gives Lyapunov stability criterion in each coordinate direction. If $d\phi_\xi < 0$, then the system is stable in that parameter, and nearby families converge to a single trajectory. If instead, $d\phi_\xi > 0$, the system diverges along that direction, with similar trajectories having highly different long-term behavior. If $d\phi_\xi = 0$, then nearby trajectories remain in nearby neighborhoods, but do not converge to each other. We define the Lyapunov exponent λ_n as the n^{th} eigenvalue of $d\phi_\xi$, given explicitly as

$$\lambda_n = \lim_{t\to\infty} \frac{\ln |d\phi^t_{\xi_n}|}{t} \tag{3}$$

1.2.2 Bifurcation and Universal Behavior

Another useful method for examining the long-term behavior of chaotic systems is to consider explicitly the *positive limit set* [10] of a flow given some initial condition:

$$L^+(\xi) = \{\chi \in U | \exists \{t_i\}_1^\infty \text{ such that } \phi^{t_i}(\xi) \to \chi\} \tag{4}$$

Our treatment of Lyapunov stability gives us some intuition about the behavior of such a set. If a system is dissapative (that is $\lambda_n < 0$ for all n), then the positiive limit set of any given initial condition should be a single point, since nearby trajectories converge to a stable value in phase space. However, if the system diverges or has chaotic behavior, we expect that there will be several stable orbits, or perhaps even more exotic behavior. This behavior is best illustrated using a *bifurcation diagram*. Taking ξ_0 to be some fixed initial condition, we compute $L^+(\xi)$ for a (possibly discrete) flow at multiple values of a *chaotic parameter*. We illustrate this concept with the Zaslavaski map, which (entirely coincidentally...) coincides with a discretized, idealized version of the Bouncing Ball system used later. [7]

The Zaslavaski map has two dynamical variables, the phase θ, and the velocity v, and two chaotic parameters, which essentially amount to tuning the function F in Equation 1 to alter the eigenvalues of the linearized flow (Lyapunov Exponents). The chaotic parameters are called Γ, the gain, and ϵ, which we fix

[9] It is worth noting that if ϕ is already linear, then $\tilde{\phi} = \phi$, and points in phase space do not drift apart or move together. This is the essential role of nonlinearity in producing chaotic behavior.

to be 1, for simplicity. The equations of motion are (after fixing ϵ)

$$\theta_{i+1} = \frac{\theta_i + 2v_i}{2\pi} \mod 1 \qquad\qquad v_{i+1} = v_i + 2 * \Gamma \cos(\theta_i + 2 * v_i)$$

By iterating the map 10,000 times at 500 values of Γ evenly spaced in $(0.5, 1)$, we obtain the diagram of Figure 2, where the x-axis represents Γ, and the y-axis is $L^+((1,1))$ projected onto v. Examining the diagram at $\Gamma \sim 0.58$, (the location of the first "split"), we expect that the phase plots ought to change from having a single stable point, to two. Indeed (as we shall see), this is the case. By interpreting the phase-space variables as the Fourier symbol[10] of their physical counterparts, this convergence to two separate points likewise indicates two sharp spikes in Fourier space, where before there was only one.

One fascinating result is that the distances between these bifurcations actually follow a preset pattern which is independent of the chaotic map, provided there is only one parameter. This result is due to Feigenbaum, and explained well by Strogatz, whose lovely diagram I borrow for my own purposes. [9, pg. 372-374] Specifically, the ratio $\frac{d_n}{d_{n+1}}$ converges to Feigenbaum's second constant $\alpha = 2.5029$, and the ratio $\frac{\Delta_n}{\Delta_{n+1}} \to \delta = 4.669$.[11] The measurement and universality of these ratios is a well-established phenomenon, and can be found with a simple web search. Because of the 1-D and unimodality conditions of the ratio, they do not apply well to our experiments, as we shall see later.

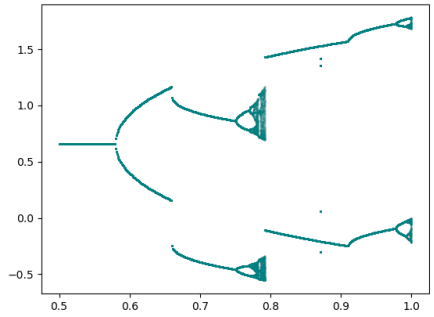

Figure 2: Bifurcation Diagram for Zaslavaski Map

1.2.3 Attractor Dimension

Finally, we discuss the dimension of an attractor, which allows us to quantify the degree to which an attractor is "strange" or self-similar. We begin first with a (very truncated[12]) discussion of measure on $\mathbb{R}^n$, emphasizing in particular the Hausdorff measure, which provides a measure-theoretic alternative to computing lower dimensional "volumes" in $\mathbb{R}^n$. We will then discuss the notion of Hausdorff *dimension*, and its relationship to self-similarity, concluding with an exposition of computationally feasible methods of computing upper bounds on the Hausdorff dimension. The motivated grader is directed to Chapter 1 of Folland's *Real Analysis* for a concise, but complete presentation of the basics of measure theory, and to Chapter 11 for a discussion of Hausdorff Measure and Dimension. The discussion of the following paragraph follows Folland quite closely. [4]

[10] See [8, pg. 99]

[11] Strogatz uses $\alpha = -2.5029$, but we will do away with this sign convention, since it is an artifact of the alternating relationship between d_{n+1} being above/below d_n.

[12] Borel who??

For a subset $U \subset \mathbb{R}^n$, we define $\text{diam}(U) = \sup_{x\in U, y\in U} |x-y|$ to be the diameter of U. We define the following function:

$$H_{p,\delta}(U) = \inf\left\{ \sum_1^\infty (\text{diam}B_j)^p \middle| U \subset \bigcup_1^\infty B_j \text{ and } \text{diam}B_j \leq \delta \right\}$$

In as many words, $H_{p,\delta}(U)$ is the minimum volume (in p-dimensions) obtained by covering U by sets with diameter less than or equal to δ. Then, the p-dimensional Hausdorff measure of U is defined as

$$H_p(U) = \lim_{\delta\to 0} H_{p,\delta}(U)$$

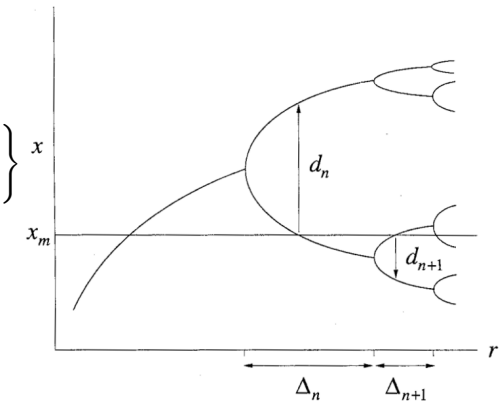

Figure 3: Illustration of Feigenbaum's Ratio by Strogatz. [9]

If we take $p = n$, on $\mathbb{R}^n$, then $\text{vol}(B_{1/2}(0))H_n(U) = m(U)$, where m is the usual Lebesgue, or volume measure. Of particular note, is that if $H_p(U) < \infty$, then for any $q > p$, $H_q(U) = 0$. Since $H_p(U) < \infty$, there exists $\delta > 0$, $\{B_i\}_1^\infty$ which covers U and has $\text{diam}B_j < \delta$. So $\sum(\text{diam}B_j)^p \leq H_p(U) + 1$, and therefore,

$$\sum(\text{diam}B_j)^q \leq \delta^{q-p}\sum(\text{diam}B_j)^p \leq \delta^{q-p}(H_p(U)+1)$$

And, since $q > p$, as $\delta \to 0$, the rightmost inequality goes to zero, and so $H_q(U) = 0$. The contrapositive also holds, that if $H_p(U) > 0$, then for any $q < p$, $H_q(U) = \infty$. So, it is clear that the "dimension" for which $H_p(U)$ is nonzero and finite is unique, and given by

$$p = \inf\{p \geq 0 | H_p(U) = 0\} = \sup\{p \geq 0 | H_p(U) = \infty\}$$

which we call the *Hausdorff Dimension* of U.[13] [4]

Computing the Hausdorff measure of an arbitrary set U computationally is essentially impossible. The central issue lies in our choice of cover $\{B_i\}$ of U, since for any set of nonzero measure, it is clear that there are countably many such covers[14] which raises the computational complexity of the presented algorithm to an unnacceptable degree. Instead, we search for numerical upper bounds on the Hausdorff (fractal) dimension of a trajectory in phase space. Here, we present two such methods for estimating the dimension of an attractor given a finite time-series sampling of a trajectory in phase space: the so-called *Box-Counting* and *Information* dimensions of an attractor. While there are numerous other estimates of Fractal dimension, and even objects such as multi-fractals, which are not well-described by any single estimate, these considerations fall beyond the scope of this paper, primarily due to length constraints. The following exposition is based

[13]The Hausdorff Dimension is also referred to as the *Fractal* dimension.

[14]Since $\mathbb{R}^n$ is second-countable. Without this nice topological separability (equivalently, it is because $\mathbb{R}^n$ has a dense, countable subset), there will certainly be uncountably many covers.

primarily on the work of Theiler. [11]

Box-Counting Dimension The difficulty in numerically computing the Hausdorff dimension of a set lies in the infimum taken over all possible covers of U. While a restriction to open subsets reduces the cardinality of the infimum without substantively changing the result (see [4]), it is difficult to prove in general that one has found the optimal cover in all cases. It is for this reason that we instead choose to cover U by open n-rectangles of side length ϵ. In this case, the Hausdorff measure H_n and the Lebesgue measure correspond with no multiplicative constant, since the volume of a rectangle with diameter (side length) 1 is in fact, 1. It is easy to see that for side length ϵ, the volume of the cover will simply be $N_\epsilon(U)$, the number of nonempty boxes, times the volume of each rectangle ϵ^n. For this reason, the Box-Counting measure of dimension p is given as

$$\mathcal{B}_{p,\epsilon}(U) = N_\epsilon(U)\epsilon^p$$

To find the value of p for which $\mathcal{B}_{p,\epsilon}$ is nonzero and finite, we require that $N_\epsilon(U) \sim \epsilon^{-p}$, which leaves a simple way to compute the box counting dimension p,

$$p_{\mathcal{B}} = \lim_{\epsilon \to 0} \frac{\ln\big(N_\epsilon(U)^{-1}\big)}{\ln(\epsilon)}$$

Information Dimension One possible caveat of the Box-Counting method is that it does not weight boxes according to their density, so it is possible that some knowledge is lost in this papering over. To remedy this situation, we introduce the normalized counting measure $\mu(B_i)$, which returns the quotient of the number of points in $U \cap B_i$, with the total number of points in U, and define the generalized, or information dimension of weight q by

$$\mathcal{I}_q(U) = \frac{1}{q-1} \lim_{\epsilon \to 0} \frac{\ln(\sum_i \mu(B_i)^q)}{\ln \epsilon}$$

It is noted by Theiler that for $q = 2$, this is the arithmetic average, and for $q = 3$, it corresponds to the root mean square. [11, pg. 1060] This quantity is called the information dimension, since it can be related to the Shannon entropy of the dynamical system, which is beyond the scope of this paper. The interested reader is directed again to Theiler.[15]

2 Experimental Apparatus

At long last, we turn to our pair of electrical models for chaotic systems: the PN-Junction, and the Bouncing-Ball circuit. In this section, we provide brief descriptions of the dynamical systems in question, and present

[15]Note: the lab manual makes an equivalence between the Lyapunov dimension and information dimension (in sec 12), yet they are nominally distinct quantities. At least from my understanding of Theiler, it is an open conjecture that the definitions of Lyapunov dimension using the eponymous coefficients coincides with the information dimension (Kaplan-Yorke conjecture). This made it onto my list of "things I wanted to study but couldn't because I had to plot data." This seems like it would be worth mentioning.

physical evidence for the results discussed in the preceding section.

2.1 PN-Junction

The first dynamical system we examined was a simple PN-junction, which consisted of a diode in series with a resistor, inductor, and a driving sine wave, as show in Figure 4. The diode is highly nonlinear. In particular, it has an exponential I-V, and even a nonlinear capacitance, which are modeled by the following [1]:

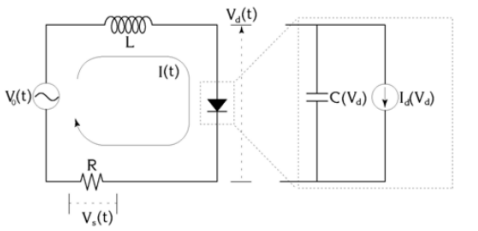

Figure 4: PN-Junction Diagram

$$C(V_d) = \begin{cases} C_0 \exp(eV_d/kT) & V_d > 0 \\ \frac{C_0}{\sqrt{1-\exp(eV_d/kT)}} & V_d \leq 0 \end{cases}$$

$$I_d(V_d) = I_0(\exp(eV_d/kT) - 1)$$

The equations of motion are given by the system of equations shown below, where $V_0(t)$ is the driving amplitude $V_0(t) = V_0(0)\cos(\omega t)$,

$$\frac{dI}{dt} = \frac{1}{L}(V_0\cos(\omega t) - RI - V) \qquad \frac{dV}{dt} = (C(V))^{-1}(I - I_d(V)) \qquad \frac{d\theta}{dt} = \omega$$

We produced bifurcation diagrams for several fixed frequencies ω by varying the chaotic parameter $V_0(t = 0)$, the amplitude of the driving force. For the sake of brevity[16] I will restrict the discussion to our results for $\omega = 4000$Hz. Upon examination of the bifurcation diagram of Figure 5, we expect that the behavior of the phase-space orbit should exhibit different topological behaviors in the intervals $(0, 2)$, $(2, 5)$, and onward. Given this intuition, we took time series data at $V_0 = 5.1$V, 7.8V, and 8.2V. Their information dimensions are reported in the table shown below. As expected, where the bifurcation diagram enters a regime resembling "dust," the estimates on the Hausdorff dimension rise noticeably.[17,18]

V_0	$\mathcal{I}_2$	$p_{\mathcal{B}}$
5.1	1.07 ± 0.01	1.12 ± 0.01
7.8	1.62 ± 0.01	1.58 ± 0.01
8.2	1.73 ± 0.01	1.67 ± 0.01

For each driving voltage, we noticed quantitatively and qualitatively different behavior corresponding to the behavior of the bifurcation diagram. Examining plots of the return map and Fourier transform further confirm our hypotheses about the qualitative behavior. The return maps in Figure 5 demonstrate both the

[16] I have another whole circuit to write about!

[17] These were computed using a linear fit, with r-correlation values greater than 0.995.

[18] This is another gripe I have with the lab manual. The manual states explicitly that the embedding map we should use is (I_n, I_{n-1}, I_{n-2}), but if we expect the Hausdorff dimension to be > 1, we ought to use 4 indices in the return map, since $2d + 1 \leq 3 \Rightarrow d \leq 1$, and we're measuring values consistently greater than 1.

period doubling and chaotic behavior as expected, with four approximate "loops" appearing in the plot for 5.1, corresponding to the four "branches" of the bifurcation diagram. In fourier space, this is confirmed as well, with four spikes,[19] one for each branch of the bifurcation diagram.

Finally, while our resolution in the Bifurcation diagram isn't great, we can still obtain a preliminary estimate of Feigenbaums constants. By reading off the graph, we estimate (using the notation of Strogatz) $\Delta_0/\Delta 1 \approx (1.8-4.9)/(4.9-7) = 1.47$, and $\Delta_1/\Delta_2 \approx (4.9-7)/(7-7.8) = 2.62$, and $d_0/d_1 = (-0.2-0.3)/(-0.2+0.1) = 5$, $d_1/d_2 = 1.6$ on the upper branch. In the $V_0 > 5$ range, we have $\alpha \approx 2$ on the lower branch, and $\alpha \approx 2.5$ on the upper. While there is not sufficient time or room in this text to examine exactly what has gone wrong with our estimate of δ, there is an obvious place to start: Feigenbaum's ratios only hold for one-dimensional, unimodal maps, which our system obviously does not satisfy. [9, Chapter 10] While I would love to delve more into the proof of the universality of these ratios, it is far outside the scope of this paper, and will require more time than I can dedicate. It is for this reason that I will also omit the measurement from the upcoming discussion of the Bouncing Ball circuit.

2.2 Bouncing Ball

The final dynamical system we explore is that of the Bouncing Ball circuit. This circuit (to which a schematic was not available) is meant to model the action of bouncing a ball on a table which oscillates at a known frequency and amplitude. In this idealized setup, we may reduce the equations of motion of the Bouncing Ball dynamical system to the Zaslavasky map under iteration, by making the gain $\Gamma = \frac{A\omega^2}{g}$, where A is the amplitude of the table oscillation, ω the driving frequency, and $g = 9.81$. [7] This map is distinct from the flow for the PN-junction, since there are numerous forbidden configurations from the dynamics of the system, which causes discontinuities in the bifurcation map, and sudden jumps in the return map. In the data presented below, we fix $\omega = 190$Hz, and vary the driving amplitude between 0 and 5 volts.

In the bifurcation diagram of Figure 6, there are a few characteristic features which we would like to consider.[20] Specifically, we would like to validate that when Γ (appropriately normalized so that it corresponds to the graph. All of these constants mean nothing to the topology of the system, since any constant multiple of one metric is topologically equivalent to any other) is in the apparent "island of stability" at (2.5,2.8), and the smaller one near 3.6, we see that the oribits are stable as well.

[19] Up to time reversal, which is fine since our system is confirmed *not* dissapative.

[20] My power went out while I was writing this part, and I lost some analysis + code (have I mentioned that I LOVE PG&E?).

Γ	$\mathcal{I}_2$	$p_{\mathcal{B}}$
0.5	0.85	0.08
1.6	0.94	0.59
1.7	1.11	0.77
2.0	1.14	1.41
2.2	1.65	1.58
3.0	1.68	1.58
4.5	1.09	1.05
5.3	1.74	1.43

At values which appear chaotic on the bifurcation diagram, we see a correspondence of higher information dimension, which aligns qualitatively with our expectation.

2.3 Sources of Error in Dimension

Our computation of the information and box dimensions of our attractors is suspect and may, in some cases, be underestimates of the true Hausdorff dimension. This is uniquely problematic, since it negates our interpretation of the box and information dimensions as upper bounds on the Hausdorff dimension. I discuss possible causes below, and further sources may be found in the discussion by Theiler. First, our estimates for highly stable trajectories are virtually guaranteed to be underestimates of the actual Hausdorff dimension. One source of error is a quirk of Takens' embedding method, which for non self-intersecting manifolds, will raise the dimensionality of the embedding to a degree where our estimates become dominated by the high dimension of the ambient space. Theiler characterizes this error in the context of nonchaotic attractors as arising from the strong correlation of sampled points. [11] Implicit in the construction of the normalized counting measure $\mu(B_i)$ is that points in B_i are noncorrelated, and that we can interpret μ as being a good measure of probability. In the case of a stable, one-dimensional limit cycle, this assumption fails, since nearby points are correlated to each other by the flow modulo the period of the orbit.

Another possibly large source of error is due to using too fine-grained a cover of our fractal. Naively, we used a sequence of $\epsilon_n = R/n$, where R was the bounding box of the measured quantities. While this does converge to zero, it does not take into account the finite nature of our measurement. Indeed, for $r = \frac{R}{\min_n(\epsilon_n)}$, we should have for N measurements that $N^2/2 \geq R^d$. [11] Checking this explicitly in our algorithm ran beyond the time assigned for the paper, but in the future, the algorithm presented in the appendix should use this as a bound for our box cover.[21]

[21]It is worth noting that the VI in lab also didn't account for this, which can be seen by the flat region for large $\ln(\epsilon)$. A better, more computationally efficient VI would account for this estimation limt A-priori and not compute values above it.

3 Conclusion

In conclusion, while we accomplished a strong qualitative characterization of the behavior of our chaotic apparatuses, a reliable quantitative measurement of the topological characterisitcs of their flows was not attained. Some of the sources of error were discussed in the previous section, and others have been omitted for the sake of brevity. Rather, the focus of this lab (and this paper), was on learning as much as feasible in the time available about the characteristics of solutions of dynamical systems, and making a first pass at measuring them from an experimental apparatus. With more time, numerous fixes have been suggested (e.g. more specialized embedding dimension, fixes to dimension estimate), which if implemented, would yield significantly more robust results.

References

[1] NLD - Non-Linear Dynamics and Chaos. http://experimentationlab.berkeley.edu/sites/default/files/writeups/NLD.pdf.

[2] Vladimir Arnold and Yulij Ilyashenko. Ordinary Differential Equations. In Vladimir Arnold and Dimitri Anosov, editors, *Dynamical Systems I*. Springer-Verlag, 1987.

[3] Connor Duncan. Math 141 Lecture Notes. Instructor: Ivan Danilenko.

[4] Gerald B. Folland. *Real Analysis: Modern Techniques and Applications*. 2009.

[5] Marco Giunti and Claudio Mazzola. *Dynamical Systems on Monoids: Toward a General Theory of Deterministic Systems and Motion*, pages 173–185. 03 2012.

[6] Victor Guillemin and Allan Pollack. *Differential Topology*. American Mathematical Society, 1974.

[7] Marcus V. Carniero Joaquim J. Barroso and Elbert E.N. Macau. Bouncing ball problem: Stability of the periodic modes. *Physical Review*, 79(2), 2009.

[8] Sung-Jin Oh. Lecture notes for math 222a. https://math.berkeley.edu/~sjoh/pdfs/notes-math222a.pdf, 2019.

[9] Steven H. Strogatz. *Nonlinear Dynamics and Chaos: With applications to physics, Biology, Chemistry and Engineering*. Perseus Books, 1994.

[10] Floris Takens. Detecting strange attractors in turbulence. In David Rand and Lai-Sang Young, editors, *Dynamical Systems and Turbulence, Warwick 1980*, pages 366–381. Springer-Verlag, Berlin, Heidelberg, 1981.

[11] James Theiler. Estimating fractal dimension. *Optical Society of America*, 7(6), June 1990.

[12] James A. Yorke Tim Sauer and Martin Casdagli. Embedology. *Journal of Statistical Physics*, 65(3-4), 1991.

A Code

Below are included the box-counting and information dimension algorithms used in our computations.

Time-Delay (3d) Our implementation of the time-delay map in 3d.

```
def time_delay(ts):
    x = ts[:-2]
    y = ts[1:-1]
    z = ts[2:]

    return x, y, z
```

Box Counting Our implementation of the Box-Counting Measure:

```
def box_count(time_series, n):
    time_series -= min(time_series)
    x = time_series[:-2]
    y = time_series[1:-1]
    z = time_series[2:]

    bounds = (np.min(time_series), np.max(time_series))
    r = (bounds[1]-bounds[0])/n
    nonempty = []
    for i in range(len(x)):
        nx = math.floor(x[i]/r)
        ny = math.floor(y[i]/r)
        nz = math.floor(z[i]/r)
        nonempty.append(int(f'{nx}{ny}{nz}'))
    N = len(np.unique(nonempty))
    return N, r
```

Information Dimension Our implementation of the Information Measure of order q.

```
def info_dim(ts, order, q):
    if q == -1:
        return box_count(ts, order)

    #ts -= min(ts)
    x,y,z = time_delay(ts)
    bounds = (np.min(ts)-0.1, np.max(ts)+0.1)
    r = (bounds[1]-bounds[0])/order
    total = len(ts)
    boxcount = np.zeros((order,order,order))
    for i in range(len(x)):
        nx = math.floor(x[i]/r)
        ny = math.floor(y[i]/r)
        nz = math.floor(z[i]/r)
        boxcount[nx,ny,nz] +=1
    boxcount = boxcount/total
    p_tot = np.sum(boxcount.ravel()**q)
    return p_tot, r
```

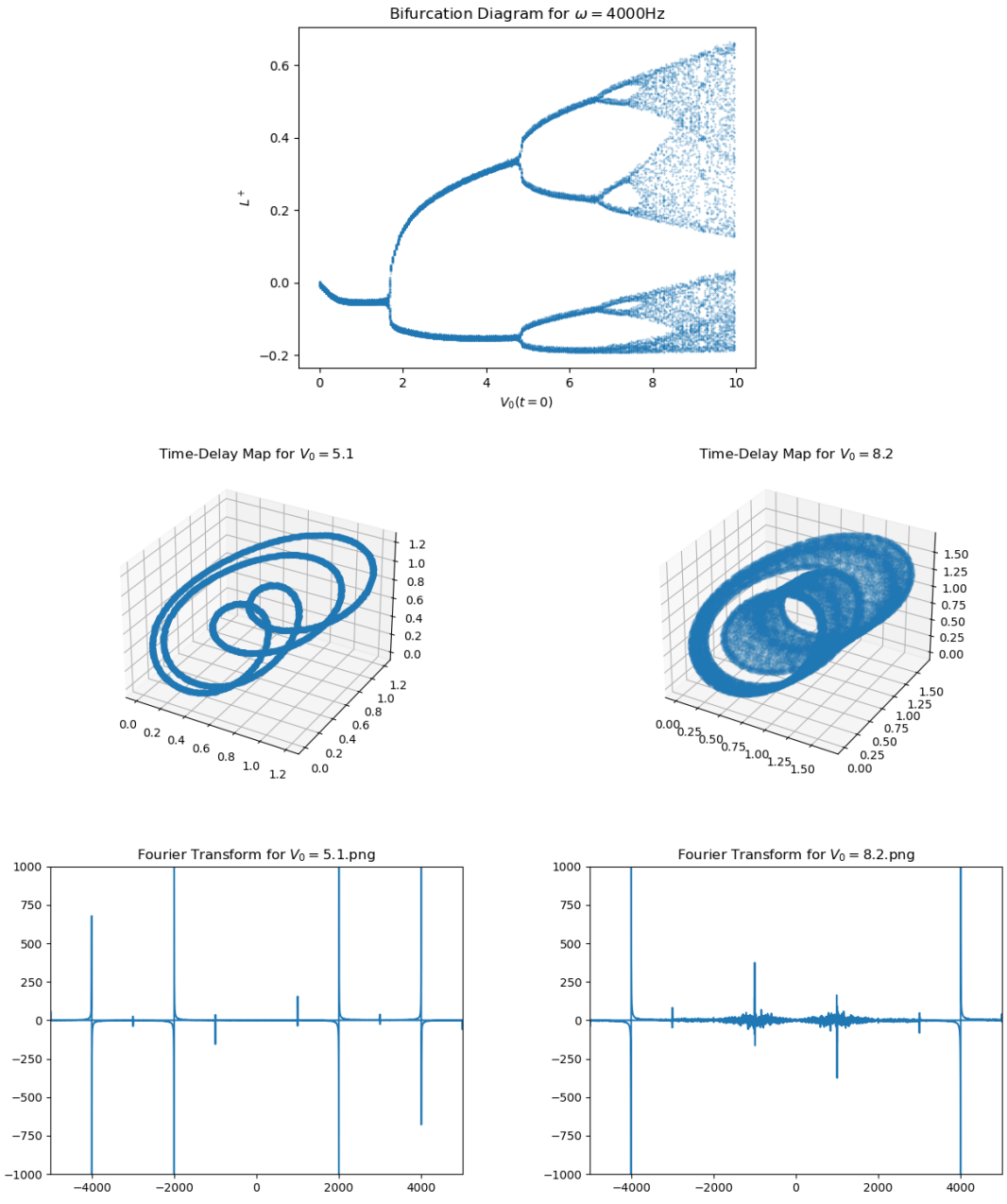

Figure 5: Bifurcation Diagram and Return maps for V_0

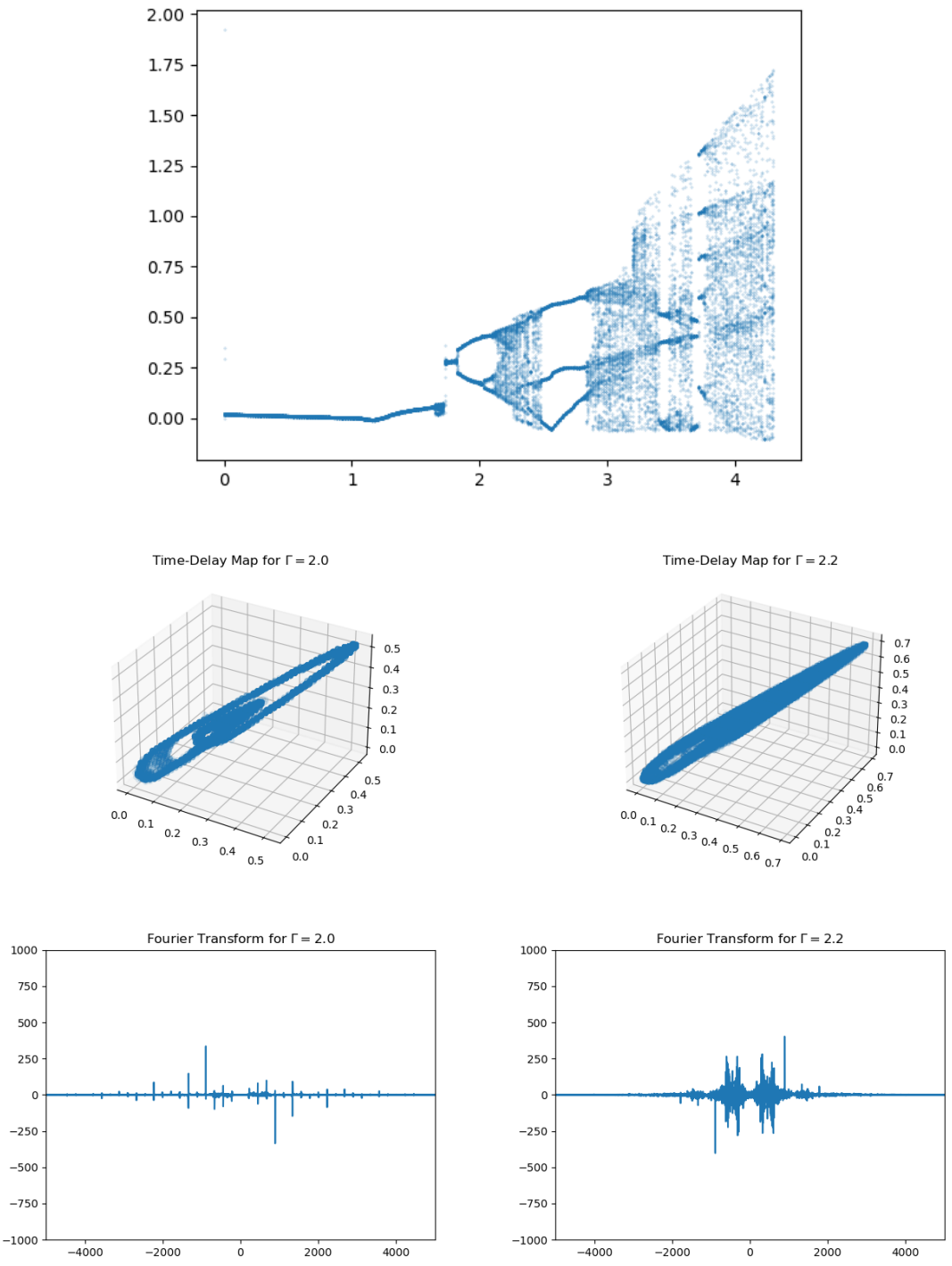

Figure 6: Bifurcation Diagram and Return Maps for the Bouncing-Ball circuit